

# Robust Secure Precoding for UAV-Aided Multi-beam Satellite NOMA Communications

Mengyan Huang, Guo Li, *Member, IEEE*, Fengkui Gong, *Member, IEEE*, Nan Zhang, *Member, IEEE*, Zhisheng Yin, *Member, IEEE*, Xingwang Li, *Senior, IEEE*, Arumugam Nallanathan, *Fellow, IEEE* and Zhiguo Ding, *Fellow, IEEE*

**Abstract**—The wide coverage and broadcasting characteristics of satellite communications lead to multi-beam downlinks being vulnerable to security threats, such as eavesdropping, hacking and illegal access. This paper takes into account the case of multiple users and an eavesdropper (Eve) in the target beam. In particular, we consider the deployment of an unmanned aerial vehicle to generate artificial noise in order to confuse Eve, while acting as a relay for the legitimate users. In addition, a non-orthogonal multiple access (NOMA) strategy is used to support multi-user communication and to improve the transmission rate. Considering the constraints due to quality of service, total and per-beam transmit power of the satellite, two robust secure precoding algorithms are presented to maximize the minimal achievable secrecy rate of the legitimate users for both non-critical and critical applications. Since the formulated optimization problems are non-convex, we first use the arithmetic-geometric mean inequality to solve the non-convex constraint of the successive interference cancellation decoding order, and the logarithmic parameter form is addressed by using the first-order Taylor series expansion. Besides, the secure outage probability constraint of the critical case is effectively resolved by applying the Bernstein-type inequality/decomposition-based large deviation inequality. Moreover, semi-definite relaxation and penalty function optimization methods are adopted to design the transmit power of the satellite in two cases, respectively. Simulation results verify the effectiveness and superiority of the proposed robust precoding design methods.

**Index Terms**—Multi-beam satellite communication, precoding, physical layer security, unmanned aerial vehicle, non-orthogonal multiple access.

## I. INTRODUCTION

Multi-beam satellite communication (SatCom) networks are considered essential in 6G due to their high data rate transmission and spectrum reuse [1]. Specifically, a

M. Huang, G. Li (corresponding author), F. Gong and N. Zhang are with State Key Laboratory of Integrated Services Networks and School of Telecommunications Engineering, Xidian University, Xi'an, China (email:my\_huang@stu.xidian.edu.cn, gli@xidian.edu.cn, fkgong@xidian.edu.cn, nzhang@xidian.edu.cn).

Z. Yin is with State Key Laboratory of Integrated Services Networks and School of Cyber Engineering, Xidian University, Xi'an, China (e-mail: zsyin@xidian.edu.cn).

X. Li is with the School of Physics and Electronic Information Engineering, Henan Polytechnic University, Jiaozuo, China (e-mail:lixingwangbupt@gmail.com).

A. Nallanathan is with the School of Electronic Engineering and Computer Science, Queen Mary University of London, London, UK (email: a.nallanathan@qmul.ac.uk).

Z. Ding is with Department of Electrical Engineering and Computer Science, Khalifa University, Abu Dhabi, UAE, and Department of Electrical and Electronic Engineering, University of Manchester, Manchester, UK (email: zhiguo.ding@manchester.ac.uk).

satellite generates multiple spot beams simultaneously through the feeder reflector antennas, where each beam covers a specific area [2]. However, satellite-terrestrial integrated network (STIN) downlinks are vulnerable to security threats because of their inherent broadcast nature and wide coverage. Attackers and eavesdroppers (Eves) within the satellite coverage are particularly difficult to be tackled, as they can hide in highly complicated environments [3]. Traditionally, secure communications have been achieved by relying on upper-layer encryption techniques [4]. Nevertheless, with the emergence of new technologies, such as cloud computing and quantum computing, this conventional security solution faces significant challenges.

Physical layer security (PLS), which exploits the inherent randomness of the wireless communication channel to protect information from eavesdropping, is regarded as an effective complementary solution to support data encryption compared to the upper layer security methods [5]–[8]. Precoding/beamforming (BF) has been widely used in specific communication scenarios since it can simultaneously increase the power of signals received by legitimate users and suppress signal leakage from unauthorized users, which is the reason why it has been recognized as an important means of enhancing the security of wireless systems. However, designing an optimal beamformer to ensure secure communications remains challenging. Recently, researchers have made considerable efforts to design secure precoding algorithms based on terrestrial and SatCom systems [9]–[13]. More specifically, the authors of [9] investigated the secrecy performance of amplify-and-forward (AF) relay terrestrial communication networks and provided a strategy in which the BF vector is a linear combination of the energy and information BF vectors. The authors of [10] studied a novel aerial BF relay system that utilized an unmanned aerial vehicle (UAV) assisted virtual antenna array to enable secure communications between remote terrestrial users (GUs). Considering satellite carries multi-antenna, joint BF of satellite and BS is proposed to achieve the positive secrecy rate of STINs [11]. Furthermore, the security problem of multi-beam SatCom systems was extended in [12], in which a suboptimal BF algorithm based on zero-forcing (ZF) and an optimal BF scheme utilizing a combination of semi-definite relaxation (SDR) and gradient methods were presented, respectively. Lin and Zhu *et al.* [13] addressed the secure problem of wirelessly powered cognitive STIN, where discretization and Taylor expansion were used to solve the non-convex problem, and then an iterative algorithm was

proposed to obtain suboptimal BF vector.

Another prospective approach for realizing secure communications is the artificial noise (AN) technique, which is to inject appropriate pseudo-random noise into the transmit signal to interfere with Eve, thus achieving an increased secrecy rate (SR) of the system. This concept was originally proposed in [14], where the AN is chosen to be in the null space of the legitimate channel, so that no interference is introduced to the legitimate receiver. The authors of [15] exploited both inherent multi-user interference and AN to enhance the security of terrestrial communication networks, and designed a power allocation (PA) strategy to maximize the achievable secrecy rate (ASR). Moreover, Xie and Zhu *et al.* [16] designed an AN-assisted ZF synthesis method to analyze the secure problem of wireless communication, which employed the ZF strategy closely related to the pseudo-inverse concept to simplify the calculation process of the baseband weighting vector. Based on the UAV-generated AN scheme, Yin and Jia *et al.* [17] explored the security issue by extending terrestrial communications to multi-beam SatComs.

Combining BF design with AN technology can achieve more secure information transmission. Nevertheless, it inevitably causes severe multiple access interference to a large number of communication devices as wireless communication evolves from single-user to multi-user scenarios [18]. The application of non-orthogonal multiple access (NOMA) has received much attention as it can accommodate more terminals and provide compelling performance improvements in terms of energy and spectrum efficiency [19]–[24]. Different from traditional orthogonal multiple access (OMA), co-channel interference (CCI) between users can be mitigated by successive interference cancellation (SIC) at the receivers [25]–[27]. To improve the secrecy performance, some related researches have been presented to show that terrestrial resources can be used to support SatComs and further use NOMA to guarantee PLS [28]–[31]. Specifically, the authors of [28] studied the security based on a hybrid satellite-ground cognitive network relying on NOMA, and derived the closed-form expression of intercept probability (IP). In [29], Yin *et al.* investigated the security problem considering SatCom downlinks and proposed a frequency-domain NOMA scheme to achieve positive SR. [30] combined BF design and cognitive radio technique to maximize the sum secrecy rate of a STIN system, where SatCom networks adopted the OMA scheme and terrestrial networks used the NOMA protocol. Moreover, Zhao *et al.* [31] explored the secure energy efficiency of a cognitive NOMA STIN system with mmWave communication by designing a hybrid analog/digital precoding strategy.

The above studies have shown that NOMA can effectively improve the throughput and spectrum efficiency of PLS systems for SatComs. However, most existing security analysis of NOMA-based satellite systems is based on perfect channel state information (CSI), which is unrealistic in satellite channel environments. The CSI error for signal detection leads to the non-removable residual interference, which degrades the performance of the system [22]. In particular, the transmission of CSI from device to satellite via gateway (GW) stations causes channel estimation errors (CEEs) due to delays and

errors [32]. If SatCom is conceived directly on the basis of perfect CSI for spot beam design, the secrecy performance of SatCom with precoding strategy will be degraded. Therefore, it is essential to comprehensively consider the impact of imperfect CSI on NOMA-based SatCom PLS systems.

### A. Motivations and Contributions

From the aforementioned works [18]–[20], it is known that security can be enhanced in SatCom networks by utilizing the NOMA protocol. Firstly, there is a trade-off between ensuring SIC decoding success and user channel enhancement/suppression in multi-beam satellite networks, as SIC decoding usually limits the channel strength of higher decoding priority users, which may make some legitimate channels weaker than the eavesdropping ones. Secondly, the mitigation of the CCI should be considered, where the precoding technique can work out this disadvantage [33]. Some initial works are devoted to the study on the secure transmission of multi-beam SatCom systems based on NOMA and precoding technologies [29]–[31], however 1) it is more realistic to consider the imperfect CSI in the practical satellite communication scenario in [29]; 2) the NOMA system considered in [30] is entirely focused on terrestrial networks; and 3) the previous research on the security of multi-beam satellite NOMA systems has been constrained the total transmit power of the satellite [31], which may result in unbalanced power distribution or unrealistic transmit power for individual antennas.

Motivated by the above observations, we investigate the secure transmission of multi-beam SatCom downlinks with imperfect CSI of Eve. Specifically, a NOMA scheme is used to support the communication of multiple terminals. To improve the secure transmission of downlink multi-beam SatComs, a fixed BF AF scheme is used to develop UAV in conjunction with satellite to ground links. In addition, we also consider a special case scenario where Eve is within the coverage range of the UAV and the UAV creates AN to confuse Eve. In this framework, we maximize the minimal ASR of legitimate NOMA users in a beam by optimizing the BF factor of satellite on the precisely of guaranteeing QoS and SIC decoding order of users in each beam. The main contributions of this paper are listed as follows.

- We propose a UAV-assisted multi-beam SatCom PLS framework that exploits full frequency reuse (FFR) between beams and accounts for non-negligible inter-beam/intra-beam interference. Specifically, a UAV with large communication range is used to generate AN to confuse Eve with imperfect CSI, which is also employed as a relay. To improve the secrecy performance, satellite precoding and NOMA techniques are integrated to realize the information transmissions.

- Non-critical and critical algorithms are designed for different applications. For the first case, our objective is to maximize the minimal ASR of NOMA users in a beam by optimizing the satellite's BF vector while guaranteeing the QoS requirements of each user, the SIC decoding order, and joint constraints on the total and per-beam transmit power of the satellite. For the critical case, we additionally impose secure outage probability (SOP) constraints on the optimization problem of maximizing

the minimal ASR to ensure secure transmission over fading channels in the presence of CEEs.

- To solve the non-convex problems mentioned above, we transform them into the equivalent one-dimensional search problems. First, the arithmetic-geometric mean (AGM) and the first-order Taylor series expansion are used to solve the constraints of the SIC decoding order of NOMA users and the logarithmic parameter form for the eavesdropping rate substitution, respectively. Then, the rank-one constraint in the non-critical case can be tackled by SDR method. Furthermore, we separately adopt the Bernstein-type inequality (BTI) and decomposition-based large deviation inequality (DBLDI) methods to perform the non-convex-to-convex transformation of the bounded constraint on the SOP, and then jointly tackle this problem iteratively using penalty function algorithm.

- Finally, the feasibility of the proposed secure precoding design schemes, i.e., non-critical and critical (critical-BTI and critical-DBLDI), is verified by numerical results. The simulation results not only compare the secrecy performance and computational complexity under different designs, but also analyze the impact of the SOP threshold, the number of beams, the number of legitimate users and the CEE factor on the minimal ASR of the proposed UAV-assisted multi-beam NOMA SatCom system.

The rest of this paper is organized as follows. Section II introduces the system architecture, the input and output modelling of signals, and the channel models. Section III presents the non-critical robust secure precoding design for the multi-beam SatCom system. The alternative optimization (AO) scheme for the critical case is described in Section IV. Numerical results are provided in Section V, where the secrecy performance and the computational complexity of the proposed communication system are compared. In Section VI, we summarize the research work of the whole paper.

*Notations:* Uppercase  $\mathbf{A}$  and lowercase  $\mathbf{a}$  stand for matrix and vector, respectively.  $\mathbb{E}[\cdot]$ ,  $\text{Tr}\{\cdot\}$ ,  $\Re\{\cdot\}$  and  $\lambda\{\cdot\}$  define the expectation, trace, real part and eigenvalue of a complex number or matrix, respectively.  $J_1(\cdot)$  and  $J_3(\cdot)$  are the first-kind Bessel functions of order 1 and 3, respectively.  $\nu_t \sim \mathcal{CN}(0, \delta_t^2)$  is the additive white Gaussian noise (AWGN) with mean zero and variance  $\delta_t^2$ .  $\langle \mathbf{A}, \mathbf{B} \rangle$  is equal to  $\text{Tr}(\mathbf{A}^H \mathbf{B})$ .

## II. SYSTEM MODEL

As shown in Fig. 1, we consider a multi-beam downlink PLS system using a low-earth orbit (LEO) satellite, where the satellite equipped with an array-fed reflector antenna serves  $N$  single-antenna ground users. A GW station maintains a cluster of  $M$  contiguous ground beams generated by  $M$  spot beams on board the satellite, and the  $m$ -th region contains  $N_m$  legitimate users and FFR is utilized among beams. To flexibly control the shape and number of beams, we exploit the multiple feeds per beam structure. In addition, a single-antenna Eve<sup>1</sup> with imperfect CSI in a target beam is assumed to be interested in intercepting the legitimate user working on the

<sup>1</sup>In some scenarios, an Eve with multiple antennas in satellite-terrestrial communication system may intercept information from either the source or the relay. We will set this assumption in our future work.

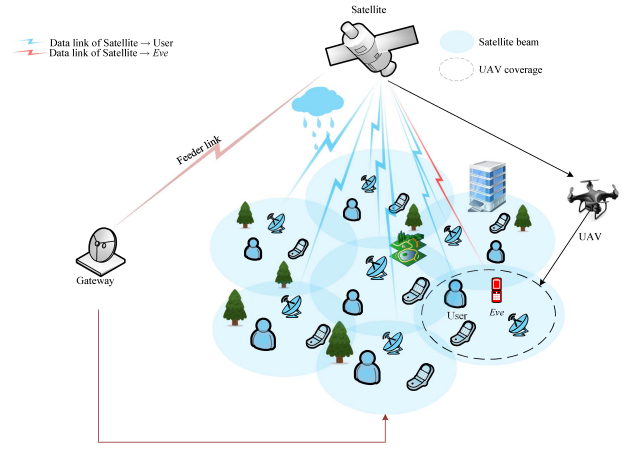


Fig. 1. UAV-assisted multi-beam LEO satellite PLS system model.

same beam. In order to achieve better secure transmission, we consider that an UAV with  $L$  antennas is deployed as a relay to improve the secure link from satellite to user, and at the same time acts as a jammer to transmit AN for confusing Eve. Furthermore, NOMA is used to support the communication of multiple widely distributed devices in the limited radio spectrum. Meanwhile, the satellite users (SUs) within an area share the same beam but decode different data streams. Similar to [17], [34], the Doppler effects in SatCom are assumed to be perfectly compensated.

### A. Transmitters

1) *Transmission signal of Satellite:* For the proposed UAV-assisted multi-beam satellite PLS system, let  $s_{m,n}$  denote the transmitted signal for  $SU_{m,n}$  with statistically normalized power. Based on NOMA protocol, the transmitted signal for the  $m$ -th beam is  $x_m = \sum_{n=1}^{N_m} \sqrt{\eta_{m,n}} s_{m,n}$ , where  $\eta_{m,n} \in [0, 1]$  is the intra-beam PA factor that can coordinate intra-beam interference and satisfy  $\sum_{n=1}^{N_m} \eta_{m,n} = 1, \forall m$ . The  $x_m$  is precoded by the precoding vector  $\mathbf{w}_m \in \mathbb{C}^{M \times 1}$  on the  $m$ -th beam to reduce inter-beam interference. Consequently, the total signal transmitted from the satellite can be expressed as

$$\mathbf{x}_S = \sum_{m=1}^M \sum_{n=1}^{N_m} \sqrt{\eta_{m,n}} \mathbf{w}_m s_{m,n}. \quad (1)$$

2) *Transmission Signal of UAV:* Without sacrificing generality, the UAV is deployed to support the secure transmission from the satellite to  $SU_{m,n}$  using full duplex operation. The UAV hovers over  $SU_{m,n}$  to receive the satellite signals while simultaneously communicating with the target user. The received signal at UAV is represented as

$$\mathbf{r}_U = \mathbf{h}_{m,l}^H \mathbf{x}_S + \nu_{m,l}, l \in \{1, 2, \dots, L\}, \quad (2)$$

where  $\mathbf{h}_{m,l} \in \mathbb{C}^{M \times 1}$  is the satellite-to-UAV channel. The AF relay protocol is used to transmit information to the legitimate user for the UAV's downlink, while the  $L \times L$  BF matrix  $\mathbf{F} = [\mathbf{f}_1, \mathbf{F}_2]$  is designed, where  $\mathbf{f}_1$  is used to send the information bearing signal and the purpose of  $\mathbf{F}_2$  is to transmit AN [35]. Therefore, the signal transmitted by UAV is described as

$$\mathbf{x}_U = \sqrt{\phi P_v} \mathbf{f}_1 \mathbf{r}_U + \sqrt{(1-\phi) P_v} \mathbf{F}_2 \mathbf{g}, \quad (3)$$

where  $P_v$  is the transmit power of the UAV.  $\phi \in [0, 1]$  represents the PA coefficient for the transmit power of the UAV. The fixed BF vector of the UAV is  $\mathbf{f}_1 \in \mathbb{C}^{L \times 1}$  with  $\|\mathbf{f}_1\|^2 = 1$ .  $\mathbf{F}_2 \in \mathbb{C}^{L \times (L-1)}$  is based on the channel vector of the UAV-to-SU $_{m,n}$ ,  $\mathbf{h}_{l,n} \in \mathbb{C}^{L \times 1}$ , which contains  $L-1$  eigenvectors of the orthogonal projection matrix  $\mathbf{I}_L - \mathbf{h}_{l,n}(\mathbf{h}_{l,n}^H \mathbf{h}_{l,n})^{-1} \mathbf{h}_{l,n}^H$  with  $\mathbf{h}_{l,n}^H \mathbf{F}_2 = \mathbf{0}$ .  $\mathbf{g} \in \mathbb{C}^{(L-1) \times 1}$  denotes the AN vector with independent identically distributed (i.i.d) elements and  $g_i \sim \mathcal{CN}(0, 1/L)$ .

## B. Channels

This subsection describes the whole communication including satellite-to-ground user/Eve, satellite-to-UAV and UAV-to-user/Eve. Due to the existence of CEEs, the channel information about Eve that are difficult to obtain perfect CSI during the actual communication process, and the most common method is to use the training sequence to estimate the channel. Thus, the channel vectors of satellite-to-Eve and UAV-to-Eve can be uniformly modelled as

$$\mathbf{h}_S = \hat{\mathbf{h}}_S + \mathbf{e}_S, S \in \{m; l, e\}, \quad (4)$$

where  $\hat{\mathbf{h}}_S$  denotes the estimated channel vector of the real channel  $\mathbf{h}_S$ .  $\mathbf{e}_S = \mathbf{E}_S^{1/2} \mathbf{v}_S$  is the corresponding stochastic channel vector measuring the CEEs with  $\mathbf{v}_m^e \sim \mathcal{CN}(0, \mathbf{I}_M)$ ,  $\mathbf{v}_{l,e} \sim \mathcal{CN}(0, \mathbf{I}_L)$ ,  $\mathbf{E}_m^e = \sigma_m^e \mathbf{I}_M$  and  $\mathbf{E}_{l,e} = \sigma_{l,e} \mathbf{I}_L$ .

1) *Satellite-to-Ground/UAV Channel*: We define the channel propagation coefficients between satellite and receiver by  $\mathbf{h}_{\bar{S}}, \bar{S} \in \{m, n; m, l\}$  and  $\hat{\mathbf{h}}_m^e$ , where  $\mathbf{h}_{m,n}^u \in \mathbb{C}^{M \times 1}$  is the channel vectors of satellite-to-SU $_{m,n}$ . We assume that there is free space loss (FSL) in the satellite-to-ground/UAV channel transmission, and the FSL coefficient is defined as [36]

$$\mathcal{C}_{S'} = \chi \sqrt{\frac{\mathcal{G}_{t,S'} \mathcal{G}_{r,S'}}{\mathcal{K}_b \mathcal{T} \mathcal{B}}}, S' \in \{m, n; m, l\}, \quad (5)$$

where  $\chi = \lambda/(4\pi d_{S'})$  represents the FSL coefficient of one receiver with  $\lambda = c/f$ ,  $d_{S'}$  is the distance between satellite and receiver,  $c$  and  $f$  are speed of light and carrier frequency, respectively.  $\mathcal{K}_b = 1.38 \times 10^{-23} \text{ J/K}$  is the Boltzman constant.  $\mathcal{T}$  and  $\mathcal{B}$  define receiver noise temperature and carrier bandwidth, respectively. Meanwhile,  $\mathcal{G}_{t,S'}$  and  $\mathcal{G}_{r,S'}$  are respectively the transmit antenna gain of the satellite and the receive beam gain of the receivers, which are denoted by

$$\mathcal{G}_{t,S'}(\theta_{S'}) = \mathcal{G}_{S'}^{\max} \left( \frac{J_1(\omega_{S'})}{2\omega_{S'}} + 36 \frac{J_3(\omega_{S'})}{\omega_{S'}^3} \right)^2 \quad (6)$$

and

$$\mathcal{G}_{r,S'} \simeq \begin{cases} \bar{\mathcal{G}}_{\max}, & 0^\circ < \phi_{S'} < 1^\circ \\ 32 - 25 \log \phi_{S'}, & 1^\circ < \phi_{S'} < 48^\circ \\ -10, & 48^\circ < \phi_{S'} \leq 180^\circ \end{cases}, \quad (7)$$

where  $\mathcal{G}_{S'}^{\max}$  denotes the maximal satellite beam gain.  $\omega_{S'} = 2.07123 \sin \theta_{S'} / \sin \theta_{S'}^{3\text{dB}}$ , in which  $\theta_{S'}$  is the angle of the corresponding receiver and beam carrier position relative to the satellite, and  $\theta_{S'}^{3\text{dB}}$  is the 3dB angle of the receiver within the  $m$ -th beam.  $\bar{\mathcal{G}}_{\max}$  represents the maximum beam gain of the boresight.  $\phi_{S'}$  expresses the angle of the off-boresight.

In addition, rain attenuation is the dominant factor in atmospheric effects and depends on the receiver location, operating frequency, polarization and elevation angle of satellite. According to ITU-R P.618 [37], the channel gain between the satellite and ground/UAV can be modelled as a log-normal random variable, i.e.,  $\ln \xi_{\text{dB}} \sim \mathcal{N}(\mu_{\xi_{\text{dB}}}, \sigma^2)$ , where  $\xi_{\text{dB}}$  denotes the channel gain,  $\mu_{\xi_{\text{dB}}}$  and  $\sigma^2$  are respectively the log-normal location and scale parameters. The satellite-to-ground/UAV rain fading vector is

$$\tilde{\mathbf{h}}_{S'} = \xi_{S'}^{-\frac{1}{2}} \exp(-j\varphi_{S'}), \quad (8)$$

where  $\varphi_{S'} \in \mathbb{C}^{M \times 1}$  represents the phase vector whose components are uniformly distributed on  $[0, 2\pi)$ .

The channel vectors of satellite-to-ground/UAV are given by

$$\mathbf{h}_{\bar{S}} = \sqrt{\mathcal{C}_{\bar{S}}} \tilde{\mathbf{h}}_{\bar{S}}, \quad (9)$$

and

$$\hat{\mathbf{h}}_m^e = \sqrt{\mathcal{C}_m^e} \tilde{\mathbf{h}}_m^e. \quad (10)$$

2) *UAV-to-Ground Channel*: The transmission from UAV to ground receiver suffers from both large-scale loss and small-scale fading [38]. The channel power gain is  $\mathcal{C}_{\mathcal{L}} = g_0 / (d_D^2 + d_H^2)$ , where  $g_0$  is the channel power gain when the reference distance is  $1m$ .  $d_D$  and  $d_H$  are respectively the horizontal distance of UAV-to-receiver and the UAV altitude. The channel vector of UAV-to-ground can be expressed as

$$\hat{\mathbf{h}}_{S^*} = \sqrt{\mathcal{C}_{\mathcal{L}}} \left( \sqrt{\frac{K_{S^*}}{K_{S^*}+1}} \tilde{\mathbf{h}}_{S^*}^{LoS} + \sqrt{\frac{1}{K_{S^*}+1}} \tilde{\mathbf{h}}_{S^*}^{Ray} \right), S^* \in \{l, n; l, e\}, \quad (11)$$

where  $\hat{\mathbf{h}}_{S^*} \in \mathbb{C}^{L \times 1}$  refers to the use of the Rician fading model for small-scale fading and  $K_{S^*}$  is Rician factor.  $\tilde{\mathbf{h}}_{S^*}^{LoS} \in \mathbb{C}^{L \times 1}$  denotes the LoS component and  $\tilde{\mathbf{h}}_{S^*}^{Ray} \in \mathbb{C}^{L \times 1}$  is the non-LoS Rayleigh fading component.  $\hat{\mathbf{h}}_{l,n} = \mathbf{h}_{l,n}$  and  $\hat{\mathbf{h}}_{l,e}$  denote the channel vector of UAV-to-SU $_{m,n}$  and the estimated channel vector of UAV-to-Eve, respectively.

## C. Receivers

We assume that the satellite-ground direct link and the UAV cooperative link arrive at the same time [17]. Due to the use of superposition coding, there is intra-beam interference between users in the same area. The terminals perform SIC to reduce CCI. Without loss of generality, we assume that the effective channel gains of the  $m$ -th beam follow an ascending order, e.g.,  $|\mathbf{h}_{m,1}^u \mathbf{w}_m|^2 \leq \dots \leq |\mathbf{h}_{m,N_m}^u \mathbf{w}_m|^2$ . Based on the NOMA protocol, the received signal of the  $n$ -th user within the  $m$ -th beam can be described by

$$\begin{aligned} y_{v_i} &= \mathbf{h}_{v_i}^H \mathbf{x}_S + \mathbf{h}_{q_i}^H \mathbf{x}_U + \nu_{v_i} \\ &= \underbrace{\mathbf{b}_{v_i} \sqrt{\eta_{m,n}} \mathbf{w}_m s_{m,n}}_{\text{Desired signal}} + \underbrace{\mathbf{b}_{v_i} \sum_{i=1, i \neq n}^{N_m} \sqrt{\eta_{m,i}} \mathbf{w}_m s_{m,i}}_{\text{Intra-beam interference}} \\ &\quad + \underbrace{\mathbf{b}_{v_i} \sum_{j=1, j \neq m}^M \mathbf{w}_j s_{j,i}}_{\text{Inter-beam interference}} + \ell_{v_i}, i \in \{1, 2\}, \end{aligned} \quad (12)$$

where  $\mathbf{b}_{v_1} = \mathbf{h}_{v_1}^H + \sqrt{\phi P_v} \mathbf{h}_{q_1}^H \mathbf{f}_1 \mathbf{h}_{m,l}^H$ ,  $\ell_{v_1} = \sqrt{\phi P_v} \mathbf{h}_{q_1}^H \mathbf{f}_1 \nu_{m,l} + \nu_{v_1}$ ,  $\ell_{v_2} = \sqrt{\phi P_v} \mathbf{h}_{q_2}^H \mathbf{f}_1 \nu_{m,l} + \sqrt{(1-\phi) P_v} \mathbf{h}_{q_2}^H \mathbf{F}_2 \mathbf{g} + \nu_{v_2}$ ,  $\{(v_1, q_1) = (u_{m,n}, l, n), (v_2, q_2) = (e_{m,l}, e)\}$ .

Here, we assume imperfect SIC to investigate the secrecy performance for the UAV-assisted SatCom NOMA system. Based on (12), the received signal-to-interference-plus-noise ratios (SINRs) at the  $n$ -th user and Eve within the  $m$ -th beam can be obtained as

$$\gamma_{v_i} = \frac{\eta_{m,n} |\mathbf{b}_{v_i} \mathbf{w}_m|^2}{\sum_{i=n+1}^{N_m} \eta_{m,i} |\mathbf{b}_{v_i} \mathbf{w}_m|^2 + \sum_{j=1, j \neq m}^M |\mathbf{b}_{v_i} \mathbf{w}_j|^2 + D_i}, \quad (13)$$

where  $D_1 = \phi P_v |\mathbf{h}_{q_1}^H \mathbf{f}_1|^2 \delta_{m,l}^2 + \delta_{m,n}^2$  and  $D_2 = \phi P_v |\mathbf{h}_{q_2}^H \mathbf{f}_1|^2 \delta_{m,l}^2 + (1-\phi) P_v |\mathbf{h}_{q_2}^H \mathbf{F}_2 \mathbf{g}|^2 + \delta_{m,e}^2$ .

According to the Shannon theorem, the channel capacity is

$$C_{v_i} = \log_2(1 + \gamma_{v_i}). \quad (14)$$

The  $n$ -th user's ASR within the  $m$ -th beam is [39]

$$C_{m,n}^{\text{ASR}} = C_{m,n}^{\text{ru}} - C_m^e. \quad (15)$$

Based on the characteristics of communication applications, i.e., non-critical and critical applications, we design two robust secure precoding algorithms for multi-beam SatCom NOMA in the presence of CEEs to maximize the minimal ASR of legitimate NOMA user in the target beam.

### III. NON-CRITICAL ROBUST SECURE DESIGN

First, we consider the case of non-critical communication applications such as agriculture, entertainment, and smart home. For these applications, the quality of the signal received over time is more important than the instantaneous one.

#### A. Problem Formulation

We aim to maximize the minimal ASR by optimizing the active BF at the satellite, while ensuring the QoS requirements of all users, the NOMA decoding order, and jointly constraining the satellite's total and per-beam transmit power. Mathematically, the optimization problem is formulated as

$$\mathcal{Q} : \max_{\mathbf{w}_m} \min_{m,n} C_{m,n}^{\text{ASR}} \quad (16a)$$

$$s.t. \quad C_{m,n}^{\text{ru}} \geq C_{m,n}^{\text{th}}, \forall m, n, \quad (16b)$$

$$C_{m,n}^{\text{ru}} \leq C_{m,k}^{\text{ru}}, 1 \leq n \leq k \leq N_m, \quad (16c)$$

$$\sum_{m=1}^M \|\mathbf{w}_m\|^2 \leq P_{\text{max}}, \|\mathbf{w}_m\|^2 \leq P_m, \forall m, \quad (16d)$$

where  $P_{\text{max}}$  and  $P_m$  are the total and per-beam transmit power of the satellite, respectively.  $C_{m,n}^{\text{th}}$  is the QoS requirement of the user terminals.

Obviously, the above problem is intractable due to its non-convexity nature, and by introducing the auxiliary variables

$R_{m,n}^{\text{ASR}}$ ,  $\alpha_{m,n}^u$ ,  $\beta_m^e$  and  $\iota_m^e$ , the original optimization problem can be transformed into

$$\mathcal{Q}_1 : \max_{\mathbf{w}_m, R_{m,n}^{\text{ASR}}, \alpha_{m,n}^u, \beta_m^e, \iota_m^e} R_{m,n}^{\text{ASR}} \quad (17a)$$

$$s.t. \quad \gamma_{m,n}^u \geq \alpha_{m,n}^u, \forall m, n, \quad (17b)$$

$$\gamma_m^e \leq \beta_m^e, \forall m, \quad (17c)$$

$$\log_2(1 + \beta_m^e) \leq \iota_m^e, \forall m, \quad (17d)$$

$$\log_2(1 + \alpha_{m,n}^u) - \iota_m^e \geq R_{m,n}^{\text{ASR}}, \forall m, n, \quad (17e)$$

$$(16b), (16c), (16d),$$

where  $R_{m,n}^{\text{ASR}} > 0$  denotes the SR threshold.

We solve  $\mathcal{Q}_1$  by importing  $\varepsilon_{m,n} = 2^{C_{m,n}^{\text{th}}} - 1$ ,  $\mathbf{W}_m = \mathbf{w}_m \mathbf{w}_m^H$ ,  $\mathbf{B}_{m,n}^u = \mathbf{b}_{m,n}^u \mathbf{b}_{m,n}^{uH}$ ,  $\mathbf{B}_m^e = \mathbf{b}_m^e \mathbf{b}_m^{eH}$ ,  $\mathbf{F}_1 = \mathbf{f}_1 \mathbf{f}_1^H$ ,  $\mathbf{F}_2 = \mathbf{F}_2 \mathbf{F}_2^H$ ,  $\mathbf{G} = \mathbf{g} \mathbf{g}^H$  and  $\mathbf{H}_{S^*} = \mathbf{h}_{S^*} \mathbf{h}_{S^*}^H$ . Substituting (13) into (17), (18) at the top of the next page can be obtained.

**Remark 1:** The problem  $\mathcal{Q}_2$  is intractable for several reasons. First, the constraints (16c), (18b), (18c) and (18d) contain fractional functions of the optimization variables. Second, (17d) is non-convex with logarithmic parameter form. Third, it is difficult to solve the rank-one constraint (18f). In order to tackle (18), some reasonable transformations and approximations are needed, as shown in the following.

#### B. Convex Transformation

To begin with, we can rewrite (18b) as

$$\text{Tr} \left( \mathbf{B}_{m,n}^u \left( \eta_{m,n} \mathbf{W}_m^{-\varepsilon_{m,n}} \sum_{i=n+1}^{N_m} \eta_{m,i} \mathbf{W}_m^{-\varepsilon_{m,n}} \sum_{j=1, j \neq m}^M \mathbf{W}_j \right) \right) \geq \varepsilon_{m,n} D_1. \quad (19)$$

Then, we import a slack variable  $z_{m,k}^u$  to solve (16c) as

$$z_{m,k}^u \leq \frac{\eta_{m,k} \text{Tr}(\mathbf{B}_{m,k}^u \mathbf{W}_m)}{\sum_{i=k+1}^{N_m} \eta_{m,i} \text{Tr}(\mathbf{B}_{m,i}^u \mathbf{W}_m) + \sum_{j=1, j \neq m}^M \text{Tr}(\mathbf{B}_{m,i}^u \mathbf{W}_j) + D_1}. \quad (20)$$

For the intractable constraint (20), we apply the AGM inequality [40] to transform it into a convex form as

$$(z_{m,k}^u \varpi_{m,k}^u)^2 + \left( \frac{\pi_{m,k}^u}{\varpi_{m,k}^u} \right)^2 \leq 2 \eta_{m,k} \text{Tr}(\mathbf{B}_{m,k}^u \mathbf{W}_m), \quad (21)$$

where the equality holds only when  $\varpi_{m,k}^u = \sqrt{\pi_{m,k}^u / z_{m,k}^u}$ ,  $\pi_{m,k}^u = \sum_{i=k+1}^{N_m} \eta_{m,i} \text{Tr}(\mathbf{B}_{m,i}^u \mathbf{W}_m) + \sum_{j=1, j \neq m}^M \text{Tr}(\mathbf{B}_{m,i}^u \mathbf{W}_j) + D_1$ . Then, exploiting (21) and **Corollary 1**, (16c) can be transformed into

$$z_{m,n}^u \leq z_{m,k}^u, 1 \leq n \leq k \leq N_m. \quad (22)$$

**Corollary 1:** When the objective function reaches the optimum, the achievable rate of the  $n$ -th user within the  $m$ -th beam decoding its own signal is  $\log_2(1 + z_{m,n}^u)$ , where

$$z_{m,n}^u = \frac{\eta_{m,n} \text{Tr}(\mathbf{B}_{m,n}^u \mathbf{W}_m)}{\sum_{i=n+1}^{N_m} \eta_{m,i} \text{Tr}(\mathbf{B}_{m,i}^u \mathbf{W}_m) + \sum_{j=1, j \neq m}^M \text{Tr}(\mathbf{B}_{m,i}^u \mathbf{W}_j) + D_1}. \quad (23)$$

$$\mathcal{Q}_2 : \max_{\mathbf{W}_m, R_{m,n}^{\text{ASR}}, \alpha_{m,n}^u, \beta_m^e, \iota_m^e} R_{m,n}^{\text{ASR}} \quad (18a)$$

$$s.t. \quad \frac{\eta_{m,n} \text{Tr}(\mathbf{B}_{m,n}^u \mathbf{W}_m)}{\sum_{i=n+1}^{N_m} \eta_{m,i} \text{Tr}(\mathbf{B}_{m,n}^u \mathbf{W}_m) + \sum_{j=1, j \neq m}^M \eta_{j,i} \text{Tr}(\mathbf{B}_{m,n}^u \mathbf{W}_j) + D_1} \geq \varepsilon_{m,n}, \forall m, n, \quad (18b)$$

$$\frac{\eta_{m,n} \text{Tr}(\mathbf{B}_{m,n}^u \mathbf{W}_m)}{\sum_{i=n+1}^{N_m} \eta_{m,i} \text{Tr}(\mathbf{B}_{m,n}^u \mathbf{W}_m) + \sum_{j=1, j \neq m}^M \eta_{j,i} \text{Tr}(\mathbf{B}_{m,n}^u \mathbf{W}_j) + D_1} \geq \alpha_{m,n}^u, \forall m, n, \quad (18c)$$

$$\frac{\eta_{m,n} \text{Tr}(\mathbf{B}_m^e \mathbf{W}_m)}{\sum_{i=n+1}^{N_m} \eta_{m,i} \text{Tr}(\mathbf{B}_m^e \mathbf{W}_m) + \sum_{j=1, j \neq m}^M \eta_{j,i} \text{Tr}(\mathbf{B}_m^e \mathbf{W}_j) + D_2} \leq \beta_m^e, \forall m, \quad (18d)$$

$$\sum_{m=1}^M \text{Tr}(\mathbf{W}_m) \leq P_{\max}, |[\mathbf{W}]_{mm}| \leq P_m, \mathbf{W}_m \succeq 0, \forall m, \quad (18e)$$

$$\text{rank}(\mathbf{W}_m) = 1, \forall m, \quad (18f)$$

$$(16c), (17d), (17e).$$

*Proof:* See Appendix A.  $\blacksquare$

For the non-convex constraints (18c) and (18d), we simplify them by introducing the auxiliary variables  $\chi_{m,n}^u$ ,  $\varphi_{m,n}^u$ ,  $\lambda_{m,n}^e$  and  $\phi_{m,n}^e$  as

$$\eta_{m,n} \text{Tr}(\mathbf{B}_{m,n}^u \mathbf{W}_m) \geq \chi_{m,n}^u, \quad (24)$$

$$\sum_{i=n+1}^{N_m} \eta_{m,i} \text{Tr}(\mathbf{B}_{m,n}^u \mathbf{W}_m) + \sum_{j=1, j \neq m}^M \text{Tr}(\mathbf{B}_{m,n}^u \mathbf{W}_j) + D_1 \leq \varphi_{m,n}^u, \quad (25)$$

$$\eta_{m,n} \text{Tr}(\mathbf{B}_m^e \mathbf{W}_m) \leq \lambda_{m,n}^e, \quad (26)$$

$$\sum_{i=n+1}^{N_m} \eta_{m,i} \text{Tr}(\mathbf{B}_m^e \mathbf{W}_m) + \sum_{j=1, j \neq m}^M \text{Tr}(\mathbf{B}_m^e \mathbf{W}_j) + D_2 \geq \phi_{m,n}^{e-1}. \quad (27)$$

In accordance with (24)-(27), (18c) and (18d) can each be further recast as

$$\alpha_{m,n}^u \varphi_{m,n}^u \leq \chi_{m,n}^u \quad (28)$$

and

$$\lambda_{m,n}^e \phi_{m,n}^e \leq \beta_m^e. \quad (29)$$

Using the AGM inequality method, the above constraints at the  $j$ -th iteration can be expressed as

$$\frac{1}{2} \left( \vartheta_{m,n}^{u(j)} \alpha_{m,n}^{u2} + \frac{\varphi_{m,n}^{u2}}{\vartheta_{m,n}^{u(j)}} \right) \leq \chi_{m,n}^u \quad (30)$$

and

$$\frac{1}{2} \left( \vartheta_{m,n}^{e(j)} \lambda_{m,n}^{e2} + \frac{\phi_{m,n}^{e2}}{\vartheta_{m,n}^{e(j)}} \right) \leq \beta_m^e, \quad (31)$$

where  $\vartheta_{m,n}^{u(j)} = \varphi_{m,n}^{u(j-1)} / \alpha_{m,n}^{u(j-1)}$  and  $\vartheta_{m,n}^{e(j)} = \phi_{m,n}^{e(j-1)} / \lambda_{m,n}^{e(j-1)}$ .  $\varphi_{m,n}^{u(j-1)}$ ,  $\alpha_{m,n}^{u(j-1)}$ ,  $\phi_{m,n}^{e(j-1)}$  and  $\lambda_{m,n}^{e(j-1)}$  denote the optimal solution of  $\varphi_{m,n}^u$ ,  $\alpha_{m,n}^u$ ,  $\phi_{m,n}^e$  and  $\lambda_{m,n}^e$  at the  $j-1$ -th iteration.

Next, we rewrite (17d) with the first-order Taylor series expansion [30], [41], [42] at  $\bar{\pi}_{m,n}^{e(j)}$

$$\log_2 \left( 1 + \bar{\pi}_{m,n}^{e(j)} \right) + \frac{\beta_m^e - \bar{\pi}_{m,n}^{e(j)}}{1 + \bar{\pi}_{m,n}^{e(j)}} \leq \iota_m^e, \quad (32)$$

where  $\bar{\pi}_{m,n}^{e(j)} = \beta_m^{e(j-1)}$  is the optimal value of the  $j$ -th iteration.

Therefore, the problem  $\mathcal{Q}_2$  of the  $j$ -th iteration can be equivalent to determining the feasibility of  $\mathbf{W}_m$ , which satisfies

$$\mathcal{Q}_3 : \text{find } \mathbf{W}_m \quad (33)$$

$$s.t. (17e), (18e), (18f), (19), (21), (22), (24) \sim (27), (30) \sim (32).$$

In addition, (18f) is the last hurdle in  $\mathcal{Q}_3$  to circumvent. Here, the constraint can be solved by using the SDR approach [43]. Therefore, the original problem can be reformulated as

$$\mathcal{Q}_4 : \max_{\mathbf{W}_m, R_{m,n}^{\text{ASR}}, \alpha_{m,n}^u, \beta_m^e, \iota_m^e, \chi_{m,n}^u, \varphi_{m,n}^u, \lambda_{m,n}^e, \phi_{m,n}^e, z_{m,n}^u} R_{m,n}^{\text{ASR}} \quad (34)$$

$$s.t. (17e), (18e), (19), (21), (22), (24) \sim (27), (30) \sim (32).$$

The above problem is concave and hence can be solved via those optimization solvers, such as CVX. Specifically, we can recover the rank-one approximate solution of the precoding problem from the higher-rank solution of the rank relaxation problem by a standard Gaussian randomization (GR) procedure, where  $\mathbf{w}_m$  is achieved from  $\mathbf{W}_m$  by using singular value decomposition (SVD). The overall algorithm is summarized in **Algorithm 1**.

Moreover, (34) includes  $11MN_m + 2M$  linear matrix inequality (LMI) constraints of dimension 1 and  $M$  LMI constraints of dimension  $M$ . Therefore, we can utilize the standard interior-point method (IPM) to explore the computational complexity of the optimization problem [44]. Given  $\tau_1 > 0$ , the number of iterations required to reach a  $\tau_1$ -optimal solution to (34) is on the order of  $-\sqrt{\Lambda_N} \ln(\tau_1)$ , where  $\Lambda_N = M(11N_m + M + 2)$  is the barrier parameter,

and  $d_N = M^3 + 6MN_m + 2M + 1 = \mathcal{O}(M^3)$  is the number of decision variables. Therefore, the complexity of a generic IPM for solving (34) is  $\zeta \ln(1/\tau_1) \sqrt{\Lambda_N} d_N [(11MN_m + 2M + M^4) + d_N(11MN_m + 2M + M^3) + d_N^2]$ , where  $\zeta$  defines the number of iterations.

---

**Algorithm 1** Non-critical Robust Secure Precoding Scheme

---

- 1: **Input:**  $M, N_m, \eta_{m,n}, C_{m,n}^{th}$  and  $SOP_{m,n}$ ;
  - 2: Initialize the feasible solutions  $\varpi_{m,k}^u, \vartheta_{m,n}^u, \vartheta_{m,n}^e$  and  $\bar{\pi}_{m,n}^e$ , and suppose  $R_{m,n}^{ASR}$  to be the optimal objective value of the  $j$ -th iteration;
  - 3: **while**  $\Delta > \tau_1$  **do**
  - 4: Solve (34) by dropping the rank-one constraint (18f), and obtain  $R_{m,n}^{ASR(j)}, \{\mathbf{W}_m^{(j)}\}_{m=1}^M, z_{m,k}^{u(j)}, \varphi_{m,n}^{u(j)}, \alpha_{m,n}^{u(j)}, \phi_{m,n}^e(j), \lambda_{m,n}^e(j), \beta_{m,n}^e(j), \varpi_{m,k}^u(j), \vartheta_{m,n}^u(j), \vartheta_{m,n}^e(j)$  and  $\bar{\pi}_{m,n}^e(j)$ ;
  - 5: Update  $\varpi_{m,k}^u = \sqrt{\frac{\pi_{m,k}^u(j)}{\pi_{m,k}^u(j-1)}}, \vartheta_{m,n}^u = \frac{\varphi_{m,n}^u(j)}{\alpha_{m,n}^u(j-1)}, \vartheta_{m,n}^e = \frac{\phi_{m,n}^e(j)}{\lambda_{m,n}^e(j)}$  and  $\bar{\pi}_{m,n}^e = \beta_{m,n}^e(j)$ ;
  - 6: **Set**  $j = j + 1$ ;
  - 7: Update  $\Delta = |R_{m,n}^{ASR(j-1)} - R_{m,n}^{ASR(j)}| < \tau_1$ ;
  - 8: **end while**
  - 9: Calculate  $\{\mathbf{w}_m^{opt}\}_{m=1}^M$  by using SVD to  $\{\mathbf{W}_m^{(j)}\}_{m=1}^M$ ;
  - 10: **Output:**  $R_{m,n}^{ASR,opt}, \{\mathbf{W}_m^{opt}\}_{m=1}^M$ .
- 

#### IV. CRITICAL ROBUST SECURE DESIGN

Then, the case of critical communication applications such as medicine, transport and industry are considered. For these applications, we impose an SOP constraint on the design of the transmit beams.

##### A. Problem Formulation

Here, the minimal ASR maximization problem is to optimize the transmit precoding vector while maintaining QoS requirements and jointly constraining the total and per-beam transmit power of the satellite. We impose an SOP constraint on the design of the minimal ASR to ensure security performance over fading channels in the presence of CEEs. The optimization problem can be expressed mathematically as

$$\mathcal{Q}^* : \max_{\mathbf{w}_m, R_{m,n}^{ASR}} R_{m,n}^{ASR} \quad (35a)$$

$$s.t. \Pr \left\{ \log_2 \left( \frac{1 + \gamma_{m,n}^u}{1 + \gamma_{m,n}^e} \right) \geq R_{m,n}^{ASR} \right\} \geq 1 - SOP_{m,n}, \quad (35b)$$

(16b), (16c), (16d),

where  $SOP_{m,n} \in (0, 1]$  is the SOP threshold of the  $n$ -th user within the  $m$ -th beam.

Similar to what we did for problem (17), we substitute (13) into (35),  $\mathcal{Q}^*$  can be rewritten as

$$\mathcal{Q}_1^* : \max_{\mathbf{W}_m, R_{m,n}^{ASR}} R_{m,n}^{ASR} \quad (36)$$

s.t. (16c), (18b), (18e), (18f), (35b).

**Remark 2:** The problem  $\mathcal{Q}^*$  is intractable for the following reasons. Firstly, (16c) and (18b) are non-convex since they are fractional functions of the optimization variables. Second, the SOP constraint (35b) contains the coupled variable. Thirdly, the rank-one constraint (18f) is difficult to handle. To solve the problem (36), an AO algorithm is proposed using the penalty function optimization method [44].

##### B. Convex Transformation

We can see that the convex transformation process of (16c) and (18b) has been shown in Section III.

For the inequality (35b), we convert it to

$$\Pr \{ \log_2(1 + \gamma_{m,n}^e) \geq \log_2(1 + \gamma_{m,n}^u) - R_{m,n}^{ASR} \} \leq SOP_{m,n}. \quad (37)$$

It can be observed that the above non-convex constraint (37) is difficult to solve as it is the difference between the two rate functions. By exploiting (22), the auxiliary variable  $t_{m,n}^e$  is introduced to simplify the probabilistic constraint (35b). Therefore, (37) can be reformulated as

$$\Pr \left\{ \frac{\eta_{m,n} \mathbf{b}_m^e \mathbf{W}_m \mathbf{b}_m^{eH}}{\sum_{i=n+1}^{N_m} \eta_{m,i} \mathbf{b}_m^e \mathbf{W}_m \mathbf{b}_m^{eH} + \sum_{j=1, j \neq m}^M \mathbf{b}_m^e \mathbf{W}_j \mathbf{b}_m^{eH} + D_2} > t_{m,n}^e \right\} \leq SOP_{m,n}. \quad (38)$$

The above inequality can be recalculated as

$$\Pr \{ \mathbf{b}_m^e \Psi_{m,n}^e \mathbf{b}_m^{eH} > t_{m,n}^e D_2 \} \leq SOP_{m,n}, \quad (39)$$

where  $\Psi_{m,n}^e = \eta_{m,n} \mathbf{W}_m - t_{m,n}^e (\sum_{i=n+1}^{N_m} \eta_{m,i} \mathbf{W}_m + \sum_{j=1, j \neq n}^M \mathbf{W}_j)$ , and  $t_{m,n}^e$  satisfies (40) at the top of the next page.

After some algebraic manipulations, (39) can be expressed as

$$\Pr \{ \mathbf{v}_m^{eH} \mathbf{Q}_m^e \mathbf{v}_m^e + 2\Re \{ \mathbf{v}_m^{eH} \mathbf{c}_m^e \} \geq \mathbf{s}_{m,n}^e \} \leq SOP_{m,n}, \quad (41)$$

where  $\mathbf{s}_{m,n}^e = t_{m,n}^e D_2 / \eta_{m,n} - \hat{\mathbf{b}}_e^{*H} \mathbf{W}_m \hat{\mathbf{b}}_e^*$ .

*Proof:* See Appendix B. ■

1) *Bernstein-Type Inequality Method:* From the above expression, the constraint is still non-convex. Fortunately, (41) can be transformed into a convex one by utilizing the BTI method [44], [45]. The deterministic form of (41) is equal to

$$\mathbf{s}_{m,n}^e \geq \text{Tr}(\mathbf{Q}_m^e) + \sqrt{2\vartheta_{m,n}} \sqrt{\|\text{vec}(\mathbf{Q}_m^e)\|_F^2 + 2\|\mathbf{c}_m^e\|^2} + \vartheta_{m,n} \lambda_{\max}^+(\mathbf{Q}_m^e), \quad (42)$$

where  $\vartheta_{m,n} = -\ln(SOP_{m,n})$ ,  $\lambda_{\max}^+(\mathbf{Q}_m^e) = \max(\lambda_{\max}(\mathbf{Q}_m^e), 0)$  with  $\lambda_{\max}(\mathbf{Q}_m^e)$  denoting the maximum eigenvalue of the matrix  $\mathbf{Q}_m^e$ .

By introducing the auxiliary variables  $\alpha_{m,n}^e$  and  $\xi_{m,n}^e$ , **Lemma 1** can be concluded as follows.

**Lemma 1: (Bernstein-Type Inequality)** The feasibility problem of (42) is given by:

$$\text{Find } \mathbf{Q}_m^e, \mathbf{c}_m^e, \mathbf{s}_{m,n}^e, \alpha_{m,n}^e, \xi_{m,n}^e$$

s.t.  $\text{Tr}(\mathbf{Q}_m^e) + \sqrt{2\vartheta_{m,n}} \alpha_{m,n}^e + \vartheta_{m,n} \xi_{m,n}^e - \mathbf{s}_{m,n}^e \leq 0, \quad (43a)$

$$\left\| \frac{\text{vec}(\mathbf{Q}_m^e)}{\sqrt{2\mathbf{c}_m^e}} \right\| \leq \alpha_{m,n}^e, \quad (43b)$$

$$\xi_{m,n}^e \mathbf{I}_M - \mathbf{Q}_m^e \succeq 0, \xi_{m,n}^e \geq 0. \quad (43c)$$

$$R_{m,n}^{\text{ASR}} \geq \log_2 \left( \frac{\eta_{m,n} \text{Tr}(\mathbf{B}_{m,n}^u \mathbf{W}_m)}{\sum_{i=n+1}^{N_m} \eta_{m,i} \text{Tr}(\mathbf{B}_{m,i}^u \mathbf{W}_m) + \sum_{j=1, j \neq m}^M \text{Tr}(\mathbf{B}_{m,n}^u \mathbf{W}_j) + D_1} \right) - \log_2(1 + t_{m,n}^e) \geq \log_2 \left( \frac{1 + z_{m,n}^u}{1 + t_{m,n}^e} \right). \quad (40)$$

Following **Lemma 1**,  $\mathcal{Q}_1^*$  can be transformed into

$$\mathcal{Q}_{BTI}^* : \max_{\substack{\mathbf{W}_m, z_{m,n}^u \\ t_{m,n}^e, \alpha_{m,n}^e, \xi_{m,n}^e}} \frac{1 + z_{m,n}^u}{1 + t_{m,n}^e} \quad (44)$$

$$s.t. \quad (18e), (18f), (19), (21), (22), (43a) \sim (43c).$$

By introducing the auxiliary variables  $\varsigma$  and  $\omega_{m,n}^e$ ,  $\max(1 + z_{m,n}^u)/(1 + t_{m,n}^e)$  can be further derived and transformed using the AGM method similar to (21) as follows

$$(\varsigma \omega_{m,n}^e)^2 + \left( \frac{1 + t_{m,n}^e}{\omega_{m,n}^e} \right)^2 \leq 2(1 + z_{m,n}^u), \quad (45)$$

where  $\omega_{m,n}^e = \sqrt{(1 + t_{m,n}^e)^{(j-1)}/\varsigma^{(j-1)}}$ .

Therefore, the above optimization problem  $\mathcal{Q}_{BTI}^*$  is equivalent to determining the feasibility of  $\mathbf{W}_m$  which satisfies

$$\mathcal{Q}_{BTI}^{*V} : \text{find } \mathbf{W}_m \quad (46)$$

$$s.t. \quad (18e), (18f), (19), (21), (22), (43a) \sim (43c), (45).$$

2) *Decomposition-Based Large Deviation Inequality Method*: In addition, (41) can be transformed to the following form by applying the DBLDI method [44]. Therefore, (41) is reformulated as

$$s_{m,n}^e \geq \text{Tr}(\mathbf{Q}_m^e) + 2\sqrt{\vartheta_{m,n}} \left( \frac{\sqrt{2}}{2} \|\mathbf{c}_m^e\| + \kappa_{m,n}^e \|\mathbf{Q}_m^e\|_F \right), \quad (47)$$

where  $\kappa_{m,n}^e > 1/\sqrt{2}$  is chosen so that  $(1 - 1/(2\kappa_{m,n}^e)^2) \kappa_{m,n}^e = \sqrt{\vartheta_{m,n}}$ .

With the introduction of auxiliary variables such as  $\alpha_{m,n}^{*e}$  and  $\xi_{m,n}^{*e}$ , **Lemma 2** can be obtained.

**Lemma 2: (Decomposition-Based Large Deviation Inequality)** The feasibility problem of (47) is given by:

$$\text{Find } \mathbf{Q}_m^e, \mathbf{c}_m^e, \mathbf{s}_{m,n}^e, \alpha_{m,n}^{*e}, \xi_{m,n}^{*e}$$

$$s.t. \quad \text{Tr}(\mathbf{Q}_m^e) + 2\sqrt{\vartheta_{m,n}} (\alpha_{m,n}^{*e} + \xi_{m,n}^{*e}) - \mathbf{s}_{m,n}^e \leq 0, \quad (48a)$$

$$1/\sqrt{2} \|\mathbf{c}_m^e\|_2 \leq \alpha_{m,n}^{*e}, \quad (48b)$$

$$\kappa_{m,n}^e \|\mathbf{Q}_m^e\|_F \leq \xi_{m,n}^{*e}, \quad (48c)$$

$$(1 - 1/(2\kappa_{m,n}^e)^2) \kappa_{m,n}^e = \sqrt{\vartheta_{m,n}}. \quad (48d)$$

Similar to  $\mathcal{Q}_{BTI}^{*V}$ , the optimization problem  $\mathcal{Q}_{DBLDI}^*$  based on the above **Lemma 2** can be equivalent to determining the feasibility of  $\mathbf{W}_m$  which satisfies

$$\mathcal{Q}_{DBLDI}^{*V} : \text{find } \mathbf{W}_m \quad (49)$$

$$s.t. \quad (18e), (18f), (19), (21), (22), (45), (48a) \sim (48d).$$

Note that  $\mathcal{Q}_{BTI}^{*V}$  and  $\mathcal{Q}_{DBLDI}^{*V}$  are still intractable due the rank-one constraint (18f). Here,  $\text{Tr}(\mathbf{W}_m) \geq \lambda_{\max}(\mathbf{W}_m)$  holds for any semi-definite matrix  $\mathbf{W}_m \succeq 0$ , and the constraint

(18f) can be rewritten as  $\text{Tr}(\mathbf{W}_m) - \lambda_{\max}(\mathbf{W}_m) \leq 0$ . This proves that  $\text{Tr}(\mathbf{W}_m) = \lambda_{\max}(\mathbf{W}_m)$ , which requires that  $\mathbf{W}_m$  have one non-zero eigenvalue only. Thus, the rank-one constraint (18f) can be equivalently expressed as

$$\text{Tr}(\mathbf{W}_m) - \lambda_{\max}(\mathbf{W}_m) \leq 0. \quad (50)$$

We find that the constraint (18f) can be guaranteed by (50) in all cases. But it is still a non-convex constraint due to the fact that  $\text{Tr}(\mathbf{W}_m) - \lambda_{\max}(\mathbf{W}_m)$  is concave. In particular,  $\lambda_{\max}(\mathbf{W}_m)$  is convex related to the Hermitian matrix. To address the problem, we adopt the penalty function approach [46] and  $\mathcal{Q}_{BTI}^{*V}$  and  $\mathcal{Q}_{DBLDI}^{*V}$  are further rewritten as

$$\mathcal{Q}_{BTI}^{*PF} : \max_{\substack{\mathbf{W}_m, \varsigma, z_{m,n}^u \\ t_{m,n}^e, \alpha_{m,n}^e, \xi_{m,n}^e}} \varsigma - \mu_m [\text{Tr}(\mathbf{W}_m) - \lambda_{\max}(\mathbf{W}_m)] \quad (51)$$

$$s.t. \quad (18e), (19), (21), (22), (43a) \sim (43c), (45)$$

and

$$\mathcal{Q}_{DBLDI}^{*PF} : \max_{\substack{\mathbf{W}_m, \varsigma, z_{m,n}^u \\ t_{m,n}^e, \alpha_{m,n}^{*e}, \xi_{m,n}^{*e}}} \varsigma - \mu_m^* [\text{Tr}(\mathbf{W}_m) - \lambda_{\max}(\mathbf{W}_m)] \quad (52)$$

$$s.t. \quad (18e), (19), (21), (22), (45), (48a) \sim (48d),$$

where  $\mu_m > 0$  and  $\mu_m^* > 0$  denote the penalty weights for the BTI and DBLDI methods, respectively<sup>2</sup>. However,  $\lambda_{\max}(\mathbf{W}_m)$  is a non-smooth function. To solve the problems further, we use the sub-gradient of the maximum eigenvalue function, which can be described as

$$\partial \lambda_{\max}(\mathbf{W}_m) = \mathbf{w}_{m,\max} \mathbf{w}_{m,\max}^H, \quad (53)$$

where  $\mathbf{w}_{m,\max}$  is the eigenvector corresponding to the maximum eigenvalue of  $\lambda_{\max}(\mathbf{W}_m)$ .

According to the above expression, we can obtain

$$\lambda_{\max}(\mathbf{W}) - \lambda_{\max}(\mathbf{W}_m) \geq \langle \mathbf{w}_{m,\max} \mathbf{w}_{m,\max}^H, \mathbf{W} - \mathbf{W}_m \rangle, \quad \forall \mathbf{W} \succeq 0. \quad (54)$$

By defining the optimal solution  $\mathbf{W}_m^{(j)}$  and computing its maximum eigenvalue and the corresponding unit eigenvector, the semi-definite problems (SDPs) are further represented as

$$\hat{\mathcal{Q}}_{BTI}^{*PF} : \max_{\substack{\mathbf{W}_m, \varsigma, z_{m,n}^u \\ t_{m,n}^e, \alpha_{m,n}^e, \xi_{m,n}^e}} \varsigma - \mu_m \left[ \text{Tr}(\mathbf{W}_m) - \lambda_{\max}(\mathbf{W}_m^{(j)}) - \langle \mathbf{w}_{m,\max}^{(j)} \mathbf{w}_{m,\max}^{(j)H}, \mathbf{W}_m - \mathbf{W}_m^{(j)} \rangle \right] \quad (55)$$

$$s.t. \quad (18e), (19), (21), (22), (43a) \sim (43c), (45)$$

<sup>2</sup>Note that if we want to obtain the optimal solutions to problems (51) and (52), the values of  $\mu_m$  and  $\mu_m^*$  should be large enough to guarantee  $\text{Tr}(\mathbf{W}_m) \approx \lambda_{\max}(\mathbf{W}_m)$ .

and

$$\hat{\mathbf{Q}}_{DBLDI}^{*PF} : \quad \max_{\mathbf{W}_m, \varsigma, z_{m,n}^u, t_{m,n}^e, \alpha_{m,n}^{*e}, \xi_{m,n}^{*e}} \varsigma - \mu_m^* \left[ \text{Tr}(\mathbf{W}_m) - \lambda_{\max}(\mathbf{W}_m^{(j)}) - \left\langle \mathbf{W}_m, \max_{\mathbf{W}_m} \mathbf{W}_m^{(j)H} \mathbf{W}_m - \mathbf{W}_m^{(j)} \right\rangle \right] \quad (56)$$

s.t. (18e), (19), (21), (22), (45), (48a) ~ (48d).

*Proof:* See Appendix C. ■

The iterative procedure is convergent from the above derivation. Therefore, (55) and (56) can be solved by a standard convex optimization software package, and the computational procedure is presented as **Algorithm 2**.

Similar to the complexity analysis in Section III, we also apply the IPM method to calculate problems (55) and (56). First, (55) contains  $6MN_m + 2M$  LMI constraints of dimension 1,  $M(N_m + 1)$  LMI constraints of dimension  $M$  and  $MN_m$  second-order cone (SOC) constraints of dimension  $M^2 + M + 1$ . Given  $\tau_2 > 0$ , the number of iterations required to obtain a  $\tau_2$ -optimal solution to (55) is of the order of  $\zeta \ln(1/\tau_2)$ , where  $\Lambda_C = M^2N_m + 8MN_m + M^2 + 2M$  is the barrier parameter, and  $d_C = M^3 + 4MN_m + 1 = \mathcal{O}(M^3)$  is the number of decision variables. Therefore, the complexity of a generic IPM for solving (55) is  $\zeta \ln(1/\tau_2) \sqrt{\Lambda_C} d_C [M^5N_m + 3M^4N_m + M^4 + 3M^3N_m + 2M^2N_m + 7MN_m + 2M + d_C(M^3N_m + M^3 + 6MN_m + 2M) + d_C^2]$ . Then, (56) has  $6MN_m + 2M$  LMI constraints of dimension 1,  $M$  LMI constraints of dimension  $M$ ,  $MN_m$  SOC constraints of dimension  $M + 1$  and  $MN_m$  SOC constraints of dimension  $M^2 + 1$ . The total computational complexity of (56) is  $\zeta \ln(1/\tau_2) \sqrt{\Lambda_C} d'_C [M^5N_m + M^4 + 3M^3N_m + 2M^2N_m + 8MN_m + 2M + d'_C(M^3 + 6MN_m + 2M) + d'_C^2]$ , where  $\Lambda'_C = 10MN_m + M^2 + 2M$  and  $d'_C = d_C$ .

## V. NUMERICAL RESULTS

TABLE I  
SYSTEM PARAMETERS [1], [10], [11], [17], [32]

The distance from satellite to receiver	$d_{S'} = 600\text{km}$
Carrier frequency	$f = 2\text{GHz}$
Carrier bandwidth	$B = 15\text{MHz}$
Receiver noise temperature	$T = 135^\circ\text{K}$
3dB angle	$\theta_{3dB} = 0.4^\circ$
Maximal beam gain	$G_{S'}^{\max} = 45\text{dB}$
Receive gain from satellite to receiver	$G_{r,S'} = 4\text{dB}$
Rain attenuation parameters	$\mu_{\xi_{dB}} = 3.125$ $\sigma^2 = 1.591$
The horizontal distance of UAV-to-receiver	$d_D = 10\text{m}$
UAV altitude	$d_H = 100\text{m}$
The number of legitimate users( $m$ -th beam)	$N_m = 2$
The number of spot beams	$M = 2$
The QoS requirements	$C_{th} = 0.1\text{bit/s/Hz}$
The Rician factor of UAV-user	$K_{l,n} = 5\text{dB}$
The Rician factor of UAV-Eve	$K_{l,e} = 0\text{dB}$

In this section, simulation results are presented to confirm the superiority of the proposed robust precoding algorithms. For simplicity, we assume that all legitimate users have the same SOP threshold ( $SOP_{m,1} = \dots = SOP_{m,N_m} = SOP_{th}$ ) and the QoS requirements ( $C_{m,1}^{th} = \dots = C_{m,N_m}^{th} = C_{th}$ ).

### Algorithm 2 Critical Robust Secure Precoding Scheme

- 1: **Input:**  $M, N_m, L, \mathbf{f}_l, \eta_{m,n}, C_{m,n}^{th}$  and  $SOP_{m,n}$ ;
- 2: Initialize  $\mathbf{W}_m^{(0)}, \varpi_{m,k}^u, \omega_{m,n}^e, R_{\min}(j-1)$  and  $R_{\min}(j)$ , and suppose  $\varsigma$  is the optimal objective value of the  $j$ -th iteration.
- 3: Set penalty function weights  $\mu_m > 0$  and  $\mu'_m > 0$ , the convergence tolerance  $\tau_2 > 0$ ;
- 4: **while**  $|R_{\min}(j-1) - R_{\min}(j)| \geq \tau_2$  **do**
- 5:   **repeat**
- 6:     Given  $j = 1$ , solve the problem (55) (or (56)) through standard software package;
- 7:     Calculate  $\mathbf{W}_m^{(j)}$  satisfying (18e), (19), (21), (22), (43a) ~ (43c), (45) (or (18e), (19), (21), (22), (45), (48a) ~ (48d)), and its maximal eigenvalue  $\lambda_{\max}(\mathbf{W}_m^{(j)})$  and corresponding eigenvector  $\mathbf{w}_{m,\max}^{(j)}$ ;
- 8:     **if**  $\mathbf{W}_m^{(j)} \approx \mathbf{W}_m^{(j-1)}$  **then**
- 9:        $\mu_m = 2\mu_m$  (or  $\mu_m^* = 2\mu_m^*$ );
- 10:     **else**
- 11:       Set  $j = j + 1$ ;
- 12:       Update  $\varpi_{m,k}^u = \sqrt{\pi_{m,k}^u(j) / z_{m,k}^u(j)}$  and  $\omega_{m,n}^e = \sqrt{(1 + t_{m,n}^e(j)) / \varsigma(j)}$ ;
- 13:     **end if**
- 14:     **until**  $|\varsigma^{*(j)} - \varsigma^{*(j-1)}| \leq \tau_2, |\text{Tr}(\mathbf{W}_m^{(j)}) - \lambda_{\max}(\mathbf{W}_m^{(j)})| \leq \tau_2, \mu_m^{(j)} \leq \mu'_m, \mu_m^{*(j)} \leq \mu'_m$ ;
- 15:     Calculate  $\{\mathbf{w}_m^{opt}\}_{m=1}^M$  by using SVD to  $\{\mathbf{W}_m^{(j)}\}_{m=1}^M$  and  $R_{m,n}^{\text{ASR},opt} = \log_2(\varsigma^{opt})$ ;
- 16:   **end while**
- 17: **Output:**  $\{\mathbf{W}_m^{(j)}\}_{m=1}^M, R_{m,n}^{\text{ASR},opt}$ .

The initialized parameters are  $\vartheta_{m,n}^{u(0)} = \vartheta_{m,n}^{e(0)} = \bar{\pi}_{m,n}^{e(0)} = \omega_{m,n}^{e(0)} = 100 * \text{ones}(M, N_m)$  and  $\varpi_{m,k}^{u(0)} = \mathbf{W}_m^{(0)} = 10 * \text{ones}(M, N_m)$  [40], [42], [45]. The PA coefficient of satellite is  $\{\eta_{m,1} = 1, N_m = 1; (\eta_{m,1}, \eta_{m,2}) = (0.6, 0.4), N_m = 2; (\eta_{m,1}, \eta_{m,2}, \eta_{m,3}) = (0.5, 0.3, 0.2), N_m = 3\}$ . The system parameters are set in Table I unless otherwise specified.

*Tag/Benchmark:* For the marked “Non-critical NOMA”, “Critical-BTI NOMA” and “Critical-DBLDI NOMA”, we consider separately non-critical and critical cases with imperfect CSI on Eve for joint precoding to ensure the communication security of the LEO satellite NOMA system. For comparisons, the “Sphere Bounding NOMA” scheme adopts the sphere bounding method to address SOP constraint based on the considered multi-beam SatCom system. In addition, considering the case of time division multiple access (TDMA), marked by “Non-critical TDMA”, “Critical-BTI TDMA”, “Critical-DBLDI TDMA” and “Sphere Bounding TDMA”, are regarded as the benchmarks.

In Fig. 2, we compare the performance of several algorithms by varying total transmit power of the satellite. The results show that the security of the non-critical precoding method is inferior to that of the critical-BTI, critical-DBLDI and Sphere

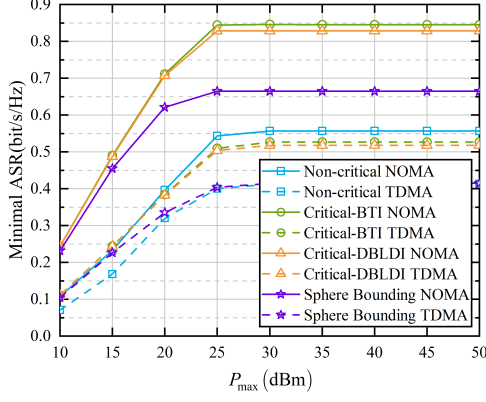


Fig. 2. Minimal ASR versus the total transmit power of satellite for different schemes ( $M = 2$ ,  $N_m = 2$ ,  $\sigma_S = 0.01$ ,  $SOP_{th} = 0.2$ ).

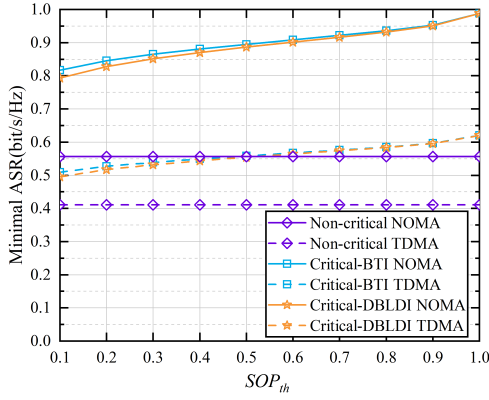


Fig. 3. Minimal ASR versus SOP threshold for different schemes ( $M = 2$ ,  $N_m = 2$ ,  $P_v = 50$ dBm and  $P_{max} = 50$ dBm).

Bounding robust algorithms, indicating that the latter methods have a strong advantage in suppressing inter-beam interference. Besides, the critical-BTI algorithm achieves the best security among these methods, followed by critical-DBLDI, and the performance difference between the critical-BTI and critical-DBLDI methods is small. Furthermore, both methods consume less energy in the critical case than the Sphere Bounding approach. The performance distinctions between the latter three algorithms are insignificant due to the weak inter-beam interference in the low signal-to-noise range. Moreover, it is obvious that TDMA has the worst security among all schemes. Although there is no interference between users in the OMA scheme, each user requires a higher transmit power than in the NOMA strategy to meet the SINR constraint.

Fig. 3 studies the secrecy performance comparison between the proposed and traditional precoding algorithms under various  $SOP_{th}$ . The simulation results show that the minimal ASR of the system in the critical case improves gradually with the increase of SOP threshold. This is due to the fact that the total transmit power consumption declines more slowly as  $SOP_{th}$  grows, indicating that the system performance under

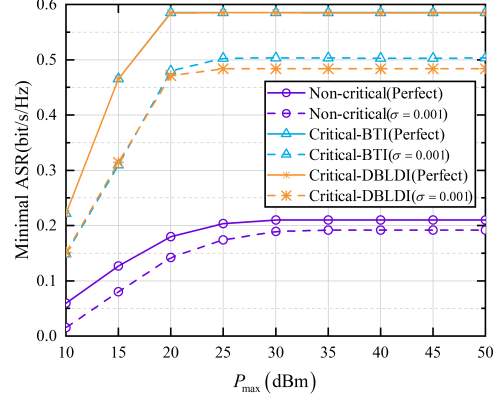


Fig. 4. Minimal ASR versus the total transmit power of satellite for different schemes ( $M = 2$ ,  $N_m = 2$ ,  $P_v = 40$ dBm).

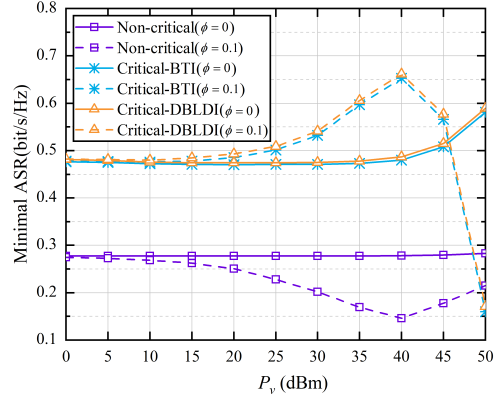


Fig. 5. Minimal ASR versus the transmit power of UAV for different  $\phi$  ( $M = 2$ ,  $P_{max} = 50$ dBm).

the critical case is more sensitive to the SOP in the restricted area. In addition, this figure also depicts that the system security of the non-critical case is maintained when  $SOP_{th}$  changes, because the non-critical algorithm is not constrained by the SOP threshold. Owing to the requirements of QoS, the SOP cannot be allowed to be too high in practical applications. Besides, it can also be seen that TDMA has the worst secure performance among all schemes.

In Fig. 4, we investigate how the performance of the proposed precoding algorithms varies with CEE factor. The simulation results are consistent with the theoretical analysis, i.e., the system's minimal ASR decreases with the CEE factor rises. Besides, the critical algorithm is more robust for the slight variation between  $\sigma = 0$  and  $\sigma = 0.001$ . The non-critical algorithm performs worse security than the critical method as  $\sigma$  increases, because the average SINR constraint is more relaxed than the SOP constraint, which also means that the critical scheme can meet higher QoS requirements.

Fig. 5 illustrates the influence of different UAV's transmit power on the system secrecy performance under the proposed robust precoding algorithms. For  $\phi = 0$ , it can be seen that the

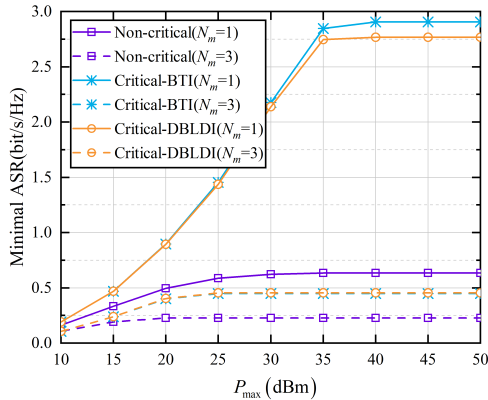


Fig. 6. Minimal ASR versus the total transmit power of satellite for different  $N_m$  ( $M = 2$ ,  $P_v = 50$ dBm).

minimal ASR of the system is proportional to  $P_v$ , especially after  $P_v = 40$ dBm. This is because the total transmit power of the UAV is used to send AN to Eve. For  $\phi = 0.1$ , we can observe that with the increase of  $P_v$ , the security in the critical case first strengthens and then weakens, as explained in the following. Although the larger  $P_v$  enhances the interference of Eve to achieve a further ascent in SR, it also causes in more disruption to legitimate receiver when at around 40dBm. For the minimal ASR in the non-critical case, the situation is reversed for the critical case. Moreover, the results show that when PA coefficient rises, the performance of the system does not necessarily get better or worse all the time, depending on the other conditions of the system.

Fig. 6 compares the minimal ASR of the non-critical and critical algorithms under different number of legitimate users. It is clear that the signal-to-noise ratio requirements of the system also grow as  $N_m$  increases, which further leads to the poor minimal ASR. Additionally, if the total transmit power is constant, a growth of  $N_m$  will reduce the transmit power from satellite to user, thereby weakening the security of the system. When there are many users, the critical-BTI and critical-DBLDI algorithms have significantly lower satellite transmit power than the non-critical method.

Fig. 7 shows the performance curves of the system as the number of beams changes. It can be seen that not only the minimal ASR of the proposed precoding algorithms decreases with the increase of  $M$ , but also the performance difference between the critical-BTI and critical-DBLDI schemes becomes smaller and smaller, which is due to more inter-beam interference introduced by the growing number of beams. The optimization results also show that the minimal ASR of the proposed algorithms becomes gradually stable with the growth of  $M$ . In particular, more beams will make the performance of the three schemes more similar.

Fig. 8 demonstrates how the computational complexity of the system varies with  $N_m$ . We can see that the computational complexity increases with the expansion of the number of legitimate users, among which the complexity of the critical-BTI scheme is the highest, and the critical-DBLDI method

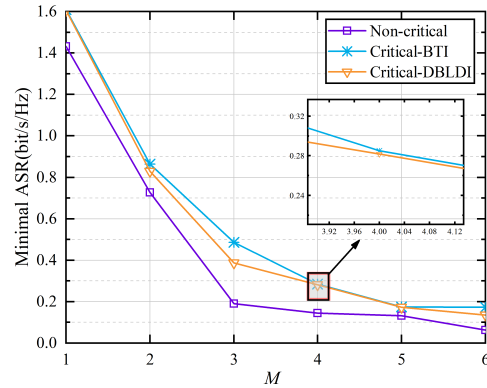


Fig. 7. Minimal ASR versus the number of satellite beams for different schemes ( $N_m = 2$ ,  $P_{\max} = 50$ dBm,  $P_v = 40$ dBm).

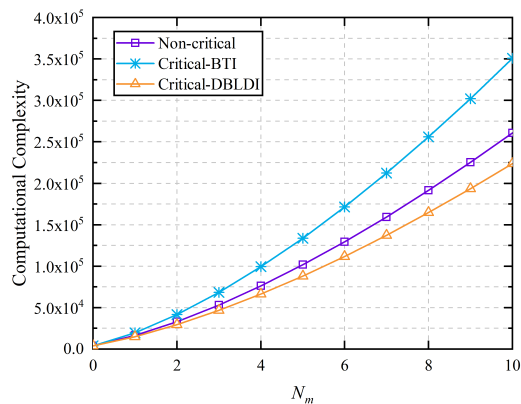


Fig. 8. Computational complexity versus  $N_m$  for different schemes with  $M = 2$ .

is the lowest. This is because the approximation based on the critical-DBLDI scheme contains only SOC constraints and thus solves more efficiently than the approximation of the critical-BTI algorithm. Particularly, the use of the critical-BTI-based approximation is more costly in terms of computational complexity and feasibility when the size of the LMI constraint is large. In contrast, the non-critical case has a higher complexity than the critical-DBLDI method because it requires more LMIs.

## VI. CONCLUSION

In this paper, we have studied the secure transmission for UAV-assisted multi-beam SatCom scenario. In the case of imperfect CSI of Eve, the minimal ASR of NOMA users in the target beam is maximized by optimizing the BF factor of the satellite. In addition, two robust secure precoding algorithms have been proposed for non-critical and critical cases according to different communication applications. Firstly, we have formulated a minimal ASR maximization problem by jointly considering the constraints of QoS, the NOMA decoding order, total and per-beam transmit power of the satellite. Then, we

have imposed the SOP constraint on the optimization problem of maximizing the minimal ASR to ensure secure transmission. To solve the non-convex problems, we have utilized the AGM inequality to transform the non-convex constraint of the SIC decoding order, and the logarithmic parameter form for the eavesdropping rate substitution has been solved by adopting the first-order Taylor series expansion. Moreover, the SOP constraint has been effectively addressed by applying the BTI/DBLDI. Furthermore, the semi-definite relaxation and the penalty function optimization methods have been used to design the transmit power of the satellite in two cases, respectively. Numerical results verified the effectiveness and robustness of the proposed algorithms.

## VII. FUTURE WORK

In future work, multi-antenna Eve can be introduced into our SatCom system to further investigate the secrecy performance. In addition, our analysis can be extended to the jointly optimize the satellite's transmit precoding vector and AN matrix, which are set as our future work.

### APPENDIX A THE PROOF OF (23)

According to the asymptotic approximation in (20), we can obtain  $z_{m,n}^u \leq \frac{z_{m,n}^{u[\max]}}{z_{m,n}^u} = \frac{\eta_{m,n} \text{Tr}(\mathbf{B}_{m,n}^u \mathbf{W}_m)}{\sum_{i=n+1}^{N_m} \eta_{m,i} \text{Tr}(\mathbf{B}_{m,i}^u \mathbf{W}_m) + \sum_{j=1, j \neq m}^M \text{Tr}(\mathbf{B}_{m,n}^u \mathbf{W}_j) + D_1}$ . Alternatively, the lower bound on the secrecy rate can be derived as follows

$$f_{s,\text{lower}} = \log_2(1 + z_{m,n}^u) - \log_2(1 + t_{m,n}^e), \quad (\text{A.1})$$

where the above expression is a monotonically increasing function on  $z_{m,n}^u$ . Therefore,  $f_{s,\text{lower}}$  becomes optimal as the objective function converges to the maximum, that is  $z_{m,n}^u = \frac{z_{m,n}^{u[\max]}}{z_{m,n}^u} = \frac{\eta_{m,n} \text{Tr}(\mathbf{B}_{m,n}^u \mathbf{W}_m)}{\sum_{i=n+1}^{N_m} \eta_{m,i} \text{Tr}(\mathbf{B}_{m,i}^u \mathbf{W}_m) + \sum_{j=1, j \neq m}^M \text{Tr}(\mathbf{B}_{m,n}^u \mathbf{W}_j) + D_1}$ .

### APPENDIX B THE PROOF OF (41)

First, (39) can be reformulated as (B.1) at the top of the next page.

In practical transmissions, legitimate users usually possess limited signal decoding capabilities, while the potential eavesdropper may have the stronger multi-user detection and interference cancellation capacities. To this end, we adopt the worst-case assumption in PLS that Eve can cancel the co-channel interference [46]. Thus, we can write the left-hand side of (39) as

$$\Pr \left\{ \mathbf{b}_m^e \mathbf{W}_m \mathbf{b}_m^{eH} \geq \frac{t_{m,n}^e D_2}{\eta_{m,n}} \right\} \leq \text{SOP}_{m,n}. \quad (\text{B.2})$$

According to (4) in Section II, we can obtain the following

$$\begin{aligned} \mathbf{b}_m^e \mathbf{W}_m \mathbf{b}_m^{eH} &= (\mathbf{h}_m^{eH} + \sqrt{\phi P_v} \mathbf{h}_{l,e}^H \mathbf{f}_1^H \mathbf{h}_{m,l}^H) \mathbf{W}_m (\mathbf{h}_m^e + \sqrt{\phi P_v} \mathbf{h}_{m,l} \mathbf{f}_1^H \mathbf{h}_{l,e}) \\ &= (\hat{\mathbf{b}}_m^* + \mathbf{e}_S)^H \mathbf{W}_m (\hat{\mathbf{b}}_m^* + \mathbf{e}_S) \\ &= \hat{\mathbf{b}}_m^{*H} \mathbf{W}_m \hat{\mathbf{b}}_m^* + 2\Re \{ \mathbf{v}_m^{eH} \mathbf{c}_m^e \} + \mathbf{v}_m^{eH} \mathbf{Q}_m^e \mathbf{v}_m^e, \end{aligned} \quad (\text{B.3})$$

where  $\hat{\mathbf{b}}_m^* = \hat{\mathbf{h}}_m^e + \sqrt{\phi P_v} \mathbf{h}_{m,l} \mathbf{f}_1^H \mathbf{h}_{l,e}$ ,  $\mathbf{c}_m^e = (\mathbf{E}_m^{e1/2})^H \mathbf{W}_m \hat{\mathbf{b}}_m^*$  and  $\mathbf{Q}_m^e = (\mathbf{E}_m^{e1/2})^H \mathbf{W}_m \mathbf{E}_m^{e1/2}$ .

Substituting (B.3) to (B.2), the following expression can be represented as

$$\mathbf{v}_m^{eH} \mathbf{Q}_m^e \mathbf{v}_m^e + 2\Re \{ \mathbf{v}_m^{eH} \mathbf{c}_m^e \} \geq \frac{t_{m,n}^e D_2}{\eta_{m,n}} - \hat{\mathbf{b}}_m^{*H} \mathbf{W}_m \hat{\mathbf{b}}_m^*. \quad (\text{B.4})$$

By inserting (B.4) into (B.1), we can obtain (41).

### APPENDIX C THE DERIVATION OF (55) AND (56)

By assuming that  $\mathbf{W}_m^{(j)}$  is the optimal solution of the problem  $\mathcal{Q}_{BTI}^{*PF}$  at the  $j$ -th iteration, we set

$$\Phi(\mathbf{W}_m^{(j)}) = -\mu_m \left[ \text{Tr}(\mathbf{W}_m^{(j)}) - \lambda_{\max}(\mathbf{W}_m^{(j)}) \right]. \quad (\text{C.1})$$

Then, the following expressions can be calculated as

$$\begin{aligned} \Phi(\mathbf{W}_m^{(j)}) &= -\mu_m \left[ \text{Tr}(\mathbf{W}_m^{(j)}) - \lambda_{\max}(\mathbf{W}_m^{(j)}) \right] \\ &\geq -\mu_m \left[ \text{Tr}(\mathbf{W}_m^{(j)}) - \lambda_{\max}(\mathbf{W}_m^{(j-1)}) \right] \\ &\quad - \left\langle \mathbf{w}_{m,\max}^{(j)} \mathbf{w}_{m,\max}^{(j-1)H}, \mathbf{W}_m^{(j)} - \mathbf{W}_m^{(j-1)} \right\rangle \\ &\geq -\mu_m \left[ \text{Tr}(\mathbf{W}_m^{(j-1)}) - \lambda_{\max}(\mathbf{W}_m^{(j-1)}) \right] \\ &= \Phi(\mathbf{W}_m^{(j-1)}). \end{aligned} \quad (\text{C.2})$$

Then, the optimal solution of  $\mathcal{Q}_{DBLDI}^{*PF}$  at the  $j$ -th iteration is similar to the derivation above.

## REFERENCES

- [1] M. G. Schraml, R. T. Schwarz, and A. Knopp, "Multiuser MIMO concept for physical layer security in multibeam satellite systems," *IEEE Trans. Inf. Forensics Security*, vol. 16, pp. 1670–1680, 2021.
- [2] N. J. G. Fonseca and J. Sombri, "Multi-beam reflector antenna system combining beam hopping and size reduction of effectively used spots," *IEEE Antennas Propag. Mag.*, vol. 54, no. 2, pp. 88–99, 2012.
- [3] Y. Zhang, J. Ye, G. Pan, and M.-S. Alouini, "Secrecy outage analysis for satellite-terrestrial downlink transmissions," *IEEE Wireless Commun. Lett.*, vol. 9, no. 10, pp. 1643–1647, 2020.
- [4] S. Spinsante, F. Chiaraluce, and E. Gambi, "Evaluation of AES-based authentication and encryption schemes for telecommand and telemetry in satellite applications," in *SpaceOps Conference*, 2006, p. 5558.
- [5] A. D. Wyner, "The wire-tap channel," *Bell system technical journal*, vol. 54, no. 8, pp. 1355–1387, 1975.
- [6] D. Wang, B. Bai, W. Zhao, and Z. Han, "A survey of optimization approaches for wireless physical layer security," *IEEE Commun. Surveys Tuts.*, vol. 21, no. 2, pp. 1878–1911, 2019.
- [7] X. Li, Q. Wang, M. Zeng, Y. Liu, S. Dang, T. A. Tsiftsis, and O. A. Dobre, "Physical-layer authentication for ambient backscatter-aided NOMA symbiotic systems," *IEEE Trans. Commun.*, vol. 71, no. 4, pp. 2288–2303, 2023.
- [8] M. Ren, J. Chen, Y. Zhou, and L. Yang, "Exploiting UAV-emitted jamming to improve physical-layer security: A 3D trajectory control perspective," *IET Commun.*, vol. 15, no. 6, 2021.
- [9] O. Waqar, H. Tabassum, and R. Adve, "Secure beamforming and ergodic secrecy rate analysis for amplify-and-forward relay networks with wireless powered jammer," *IEEE Trans. Veh. Technol.*, vol. 70, no. 4, pp. 3908–3913, 2021.
- [10] G. Sun, J. Li, A. Wang, Q. Wu, Z. Sun, and Y. Liu, "Secure and energy-efficient UAV relay communications exploiting collaborative beamforming," *IEEE Trans. Commun.*, vol. 70, no. 8, pp. 5401–5416, 2022.
- [11] M. Lin, Z. Lin, W. Zhu, and J. Wang, "Joint beamforming for secure communication in cognitive satellite terrestrial networks," *IEEE J. Sel. Areas Commun.*, vol. 36, no. 5, pp. 1017–1029, 2018.

$$\Pr \left\{ \mathbf{b}_m^e \left( \eta_{m,n} \mathbf{W}_m - t_{m,n}^e \sum_{i=n+1}^{N_m} \eta_{m,i} \mathbf{W}_m - t_{m,n}^e \sum_{j=1, j \neq m}^M \mathbf{W}_j \right) \mathbf{b}_m^{eH} \geq t_{m,n}^e D_2 \right\} \leq SOP_{m,n}, \quad (\text{B.1})$$

- [12] G. Zheng, P.-D. Arapoglou, and B. Ottersten, "Physical layer security in multibeam satellite systems," *IEEE Trans. Wireless Commun.*, vol. 11, no. 2, pp. 852–863, 2012.
- [13] Z. Lin, M. Lin, W.-P. Zhu, J.-B. Wang, and J. Cheng, "Robust secure beamforming for wireless powered cognitive satellite-terrestrial networks," *IEEE Trans. Cog. Commun. Network.*, vol. 7, no. 2, pp. 567–580, 2021.
- [14] S. Goel and R. Negi, "Guaranteeing secrecy using artificial noise," *IEEE Trans. Wireless Commun.*, vol. 7, no. 6, pp. 2180–2189, 2008.
- [15] H. Xia, X. Zhou, S. Han, C. Li, and Y. Chai, "Joint secure transceiver design and power allocation for AN-assisted MIMO networks," *IEEE Trans. Wireless Commun.*, vol. 21, no. 1, pp. 477–488, 2022.
- [16] T. Xie, J. Zhu, and Y. Li, "Artificial-noise-aided zero-forcing synthesis approach for secure multi-beam directional modulation," *IEEE Commun. Lett.*, vol. 22, no. 2, pp. 276–279, 2017.
- [17] Z. Yin, M. Jia, N. Cheng, W. Wang, F. Lyu, Q. Guo, and X. Shen, "UAV-assisted physical layer security in multi-beam satellite-enabled vehicle communications," *IEEE Trans. Intell. Transp. Syst.*, vol. 23, no. 3, pp. 2739–2751, 2022.
- [18] X. Liu, X. B. Zhai, W. Lu, and C. Wu, "QoS-guarantee resource allocation for multibeam satellite industrial internet of things with NOMA," *IEEE Trans. Ind. Informat.*, vol. 17, no. 3, pp. 2052–2061, 2021.
- [19] V. Bankey, V. Singh, and P. K. Upadhyay, "Physical layer secrecy of NOMA-based hybrid satellite-terrestrial relay networks," in *2020 IEEE Wireless Commun. Network. Conf. (WCNC)*, 2020, pp. 1–6.
- [20] A. I. Perez-Neira, M. Caus, and M. A. Vazquez, "Non-orthogonal transmission techniques for multibeam satellite systems," *IEEE Commun. Mag.*, vol. 57, no. 12, pp. 58–63, 2019.
- [21] Q. Wang, X. Li, S. Bhatia, Y. Liu, L. T. Alex, S. A. Khowaja, and V. G. Menon, "UAV-enabled non-orthogonal multiple access networks for ground-air-ground communications," *IEEE Trans. Green Commun. Network.*, vol. 6, no. 3, pp. 1340–1354, 2022.
- [22] Z. Wei, L. Yang, D. W. K. Ng, J. Yuan, and L. Hanzo, "On the performance gain of NOMA over OMA in uplink communication systems," *IEEE Trans. Commun.*, vol. 68, no. 1, pp. 536–568, 2020.
- [23] Y. Cai, Z. Wei, S. Hu, C. Liu, D. W. K. Ng, and J. Yuan, "Resource allocation and 3D trajectory design for power-efficient IRS-assisted UAV-NOMA communications," *IEEE Trans. Wireless Commun.*, vol. 21, no. 12, pp. 10 315–10 334, 2022.
- [24] M. Ren, J. Chen, B. He, K. Wu, Y. Zhou, X. Xue, and L. Yang, "Cooperative NOMA-MEC with helper scheduling," *IEEE Commun. Lett.*, vol. 26, no. 7, pp. 1693–1697, 2022.
- [25] L. Dai, B. Wang, Z. Ding, Z. Wang, S. Chen, and L. Hanzo, "A survey of non-orthogonal multiple access for 5G," *IEEE Commun. Surveys Tuts.*, vol. 20, no. 3, pp. 2294–2323, 2018.
- [26] H. Hacı, H. Zhu, and J. Wang, "Performance of non-orthogonal multiple access with a novel asynchronous interference cancellation technique," *IEEE Trans. Commun.*, vol. 65, no. 3, pp. 1319–1335, 2017.
- [27] Q.-V. Pham, T. Huynh-The, M. Alazab, J. Zhao, and W.-J. Hwang, "Sum-rate maximization for UAV-assisted visible light communications using NOMA: Swarm intelligence meets machine learning," *IEEE Internet Things J.*, vol. 7, no. 10, pp. 10 375–10 387, 2020.
- [28] H.-N. Nguyen, N.-L. Nguyen, N.-T. Nguyen, A.-T. Le, N. X. Ha, D.-T. Do, and M. Voznak, "Reliable and secure transmission in multiple antennas hybrid satellite-terrestrial cognitive networks relying on NOMA," *IEEE Access*, vol. 8, pp. 215 044–215 056, 2020.
- [29] Z. Yin, M. Jia, W. Wang, N. Cheng, F. Lyu, Q. Guo, and X. Shen, "Secrecy rate analysis of satellite communications with frequency domain NOMA," *IEEE Trans. Veh. Technol.*, vol. 68, no. 12, pp. 11 847–11 858, 2019.
- [30] H. Li, S. Zhao, Y. Li and C. Peng, "Sum secrecy rate maximization in NOMA-based cognitive satellite-terrestrial network," *IEEE Wireless Commun. Lett.*, vol. 10, no. 10, pp. 2230–2234, 2021.
- [31] F. Zhao, W. Hao, H. Guo, G. Sun, Y. Wang, and H. Zhang, "Secure Energy Efficiency for mmWave-NOMA Cognitive Satellite Terrestrial Network," *IEEE Commun. Lett.*, vol. 27, no. 1, pp. 283–287, 2022.
- [32] B. Zhao, M. Lin, M. Cheng, W.-P. Zhu, and N. Al-Dhahir, "Outage constrained robust secure beamforming in cognitive satellite-aerial networks," *IEEE Commun. Lett.*, vol. 25, no. 8, pp. 2708–2712, 2021.
- [33] R. T. Schwarz, T. Delamotte, K.-U. Storek, and A. Knopp, "MIMO applications for multibeam satellites," *IEEE Trans. Broadcast.*, vol. 65, no. 4, pp. 664–681, 2019.
- [34] C. Ding, J. Wang, H. Zhang, M. Lin, and G. Li, "Joint optimization of transmission and computation resources for satellite and high altitude platform assisted edge computing," *IEEE Trans. Wireless Commun.*, vol. 21, no. 2, pp. 1362–1377, 2022.
- [35] L. Lv, Z. Ding, Q. Ni, and J. Chen, "Secure MISO-NOMA transmission with artificial noise," *IEEE Trans. Veh. Technol.*, vol. 67, no. 7, pp. 6700–6705, 2018.
- [36] K. Guo, K. An, B. Zhang, Y. Huang, and G. Zheng, "Outage analysis of cognitive hybrid satellite-terrestrial networks with hardware impairments and multi-primary users," *IEEE Wireless Commun. Lett.*, vol. 7, no. 5, pp. 816–819, 2018.
- [37] P. Series, "Propagation data and prediction methods required for the design of earth-space telecommunication systems," *Recommendation ITU-R*, pp. 618–12, 2015.
- [38] W. Shi, J. Li, N. Cheng, F. Lyu, S. Zhang, H. Zhou, and X. Shen, "Multi-drone 3-D trajectory planning and scheduling in drone-assisted radio access networks," *IEEE Trans. Veh. Technol.*, vol. 68, no. 8, pp. 8145–8158, 2019.
- [39] Y. Liang, G. Kramer, and H. V. Poor, "Compound wiretap channels," *EURASIP J. Wireless Commun. Network.*, vol. 2009, pp. 1–12, 2009.
- [40] W. Zhang, J. Chen, Y. Kuo, and Y. Zhou, "Transmit beamforming for layered physical layer security," *IEEE Trans. Veh. Technol.*, vol. 68, no. 10, pp. 9747–9760, 2019.
- [41] A. Beck, A. Ben-Tal, and L. Tetrushvili, "A sequential parametric convex approximation method with applications to nonconvex truss topology design problems," *J. Global Optim.*, vol. 47, pp. 29–51, 2010.
- [42] S. Hu, Z. Wei, Y. Cai, C. Liu, D. W. K. Ng, and J. Yuan, "Robust and secure sum-rate maximization for multiuser MISO downlink systems with self-sustainable IRS," *IEEE Trans. Commun.*, vol. 69, no. 10, pp. 7032–7049, 2021.
- [43] Z.-q. Luo, W.-k. Ma, A. M.-c. So, Y. Ye, and S. Zhang, "Semidefinite relaxation of quadratic optimization problems," *IEEE Signal Process. Mag.*, vol. 27, no. 3, pp. 20–34, 2010.
- [44] K.-Y. Wang, A. M.-C. So, T.-H. Chang, W.-K. Ma, and C.-Y. Chi, "Outage constrained robust transmit optimization for multiuser MISO downlinks: Tractable approximations by conic optimization," *IEEE Trans. Signal Process.*, vol. 62, no. 21, pp. 5690–5705, 2014.
- [45] Z. Zhang, J. Chen, Q. Wu, Y. Liu, L. Lv, and X. Su, "Securing NOMA networks by exploiting intelligent reflecting surface," *IEEE Trans. Commun.*, vol. 70, no. 2, pp. 1096–1111, 2022.
- [46] X. Yu, D. Xu, Y. Sun, D. Ng, and R. Schober, "Robust and secure wireless communications via intelligent reflecting surfaces," *IEEE J. Sel. Areas Commun.*, vol. 38, no. 11, pp. 2637–2652, 2020.